

Pseudoscalar transition form factors and the hadronic light-by-light contribution to the anomalous magnetic moment of the muon from holographic QCD

Josef Leutgeb, Jonas Mager, and Anton Rebhan

*Institut für Theoretische Physik, Technische Universität Wien,
Wiedner Hauptstrasse 8-10, A-1040 Vienna, Austria*
(Dated: August 1, 2019)

We revisit the predictions for the pseudoscalar-photon transition form factors in bottom-up and top-down holographic QCD models which only use the pion decay constant and the ρ meson mass as input. We find remarkable agreement with the available experimental data for the single-virtual π^0 form factor that have recently been extended to lower momenta by BESIII, down to 0.3 GeV^2 . The bottom-up models moreover turn out to be roughly consistent with recent experimental results obtained by BaBar for the double-virtual η' form factor at large momenta as well as with a recent lattice extrapolation for the double-virtual π^0 form factor. Calculating the pion pole contribution to the hadronic light-by-light scattering in the anomalous magnetic moment of the muon, we find that the bottom-up models in question span the range $a_\mu^{\pi^0} = 5.9(2) \cdot 10^{-10}$, which is about 10% lower than estimated previously by approximating these holographic predictions through simple interpolators.

I. INTRODUCTION

The current world average for the experimental value of the anomalous magnetic moment of the muon [1], $a_\mu = (g_\mu - 2)/2$, which is dominated by the final result of the E821 collaboration at Brookhaven National Laboratory obtained 15 years ago, reads [2]

$$a_\mu^{\text{exp.}} = (11659209.1 \pm 6.3) \times 10^{-10}, \quad (1)$$

with new experiments at FERMILAB and J-PARC aiming at an even more precise determination. According to the recent update in Ref. [3], the Standard Model prediction is 3.7 standard deviations below this value, at

$$a_\mu^{\text{theory}} = (11659182.04 \pm 3.56) \times 10^{-10}, \quad (2)$$

where the uncertainty is almost entirely due to strong-interaction contributions, in particular the hadronic light-by-light (HLBL) scattering contribution. The latter is dominated by the exchange of a pseudoscalar meson, π^0 , η , or η' , due to their anomalous coupling to two photons. The crucial input in the calculation of a_μ in the so-called pion-pole approximation [4] comes from the pseudoscalar transition form factor (TFF) $F_{\pi^0\gamma^*\gamma^*}(Q_1^2, Q_2^2)$ (and analogously for η and η') at spacelike photon momenta.

$F(0,0)$ is determined by the known decay rates into two real photons. Experimental data for $F_{\pi^0}(Q^2, 0)$ in the region $Q^2 \lesssim 1 \text{ GeV}^2$, where the bulk of the pion-pole contribution to a_μ arises [5], have been obtained in particular by the CELLO collaboration [6] and recently by BESIII [7]. In the calculation of a_μ , a model of the double-virtual TFF is needed, for which data in the relevant momentum region are still lacking.

In this note we shall review a set of holographic models for (large- N_c) quantum chromodynamics (QCD) that have been studied previously [8–12] with respect to their prediction of the pseudoscalar TFF and the resulting prediction for the HLBL scattering contribution to a_μ in the pion-pole approximation [11, 12]. We compare in detail the top-down model of Sakai and Sugimoto [13, 14], which is only applicable at low momenta, and three bottom-up models, which have a simpler

construction in the infrared but reproduce qualitatively (and some also quantitatively) the short-distance constraints from perturbative QCD. All these models are completely fixed, once f_π and the mass of the ρ meson are given. Comparing with the experimental data reviewed in [7], which include preliminary low-energy data for $F_{\pi^0}(Q^2, 0)$ from BESIII, we find a surprisingly good agreement for the bottom-up models, whereas the Sakai-Sugimoto model performs well only at the lowest values of Q^2 . Compared to the interpolators used in Ref. [12] and the new one proposed by Danilkin, Redmer, and Vanderhaeghen (DRV) in [7], the holographic models unanimously predict a milder dependence on the difference $Q_1^2 - Q_2^2$ at fixed sum $Q_1^2 + Q_2^2$, which should be testable by future experiments at BESIII. In fact, the behavior found in the recent lattice extrapolation of Ref. [15] for the π^0 TFF for generic virtualities is closer to that of the holographic results than that of the DRV interpolator.

In contrast to Ref. [12], we have used directly the holographic TFF to numerically evaluate the HLBL contribution to a_μ using the full 3-dimensional integral formulae of Ref. [5], without recourse to an interpolator that permits the simplification to the 2-dimensional integral representation of Ref. [4]. Indeed, the (extended) D'Ambrosio-Isidori-Portoles (DIP) interpolator used in Ref. [12] to include one of the holographic predictions for the curvature parameters in the TFF does not permit to also fit the full UV behavior of the holographic models, missing in particular the Brodsky-Lepage constraint [16], which is respected in all bottom-up models. This turns out to lead to an over-estimation of the single-virtual TFF and, as a consequence, gives a result for a_μ that is about 10% higher. With full numerical evaluation, the bottom-up-holographic results span the range $a_\mu^{\pi^0} = 5.9(2) \cdot 10^{-10}$, which turns out to be well in line with the recent result obtained with the DRV interpolator fitted to the world data for π^0 [7] and also with the lattice results of Ref. [15].

II. HOLOGRAPHIC QCD MODELS

The AdS/CFT conjecture [17] has led to a new approach to studying strongly interacting non-Abelian gauge theories in the limit of large color number N_c . Originally formulated for superconformal field theories only, in particular for the dual pair of type-IIB supergravity on $\text{AdS}_5 \times S^5$ and four-dimensional $\mathcal{N} = 4$ super-Yang-Mills theory, it was quickly realized that this can also be employed for studying nonconformal systems. Indeed, a most fruitful application has been super-Yang-Mills theories at finite temperature, where temperature introduces a scale and also breaks supersymmetry [18]. A similar procedure was proposed by Witten [18] to model nonsupersymmetric low-energy Yang-Mills theory, namely as a circle-compactified five-dimensional super-Yang-Mills theory whose dual is the near-horizon geometry of D4 branes in type-IIA supergravity. Below the Kaluza-Klein mass scale introduced in compactifying a superfluous spatial direction, only the Yang-Mills fields remain massless. Discarding the corresponding Kaluza-Klein modes (which cannot be made arbitrarily heavy without leaving the supergravity approximation), one thus obtains a model for four-dimensional Yang-Mills theory given by type-IIA supergravity on a six-dimensional space with the topology of a Euclidean black hole, i.e., a spacetime that is cut off smoothly when the radius of the compactifying circle goes to zero.

In Ref. [13, 14] Sakai and Sugimoto succeeded in constructing a holographic dual with chiral quarks and nonabelian chiral symmetry breaking by introducing N_f probe D8 and anti-D8 branes localised in the extra dimension of the Witten model. The chiral symmetry $U(N_f)_L \times U(N_f)_R$ of separated stacks of branes is broken spontaneously to the diagonal subgroup by the necessity of connecting the D8- $\bar{\text{D}}8$ pairs in the terminating bulk geometry. The resulting model is a geometric realization of the so-called hidden local symmetry approach to chiral symmetry breaking, correctly implementing the nonabelian flavor anomalies through the Chern-Simons term of the D8-branes.

Already before this fully top-down string-theoretic construction, bottom-up models which real-

ize a confining geometry by some cutoff of the bulk geometry have been created, where the bulk flavor gauge fields are introduced by hand and a spontaneous breaking of chiral symmetry is engineered either by an extra bifundamental scalar field or by suitable boundary conditions. While the (Witten-)Sakai-Sugimoto (SS) model provides a most natural realization of the infrared phenomena of confinement and chiral symmetry breaking, it lacks a viable ultraviolet completion that would make contact to QCD at higher energies. Bottom-up models instead retain conformal symmetry in the ultraviolet and break it forcibly in the infrared.

Following Ref. [12] we shall focus on the most economical and thus also maximally predictive models which use only the pion decay constant and the mass of the ρ meson as input. In the hard-wall (HW) models, AdS₅ space with metric

$$ds^2 = z^{-2}(\eta_{\mu\nu}dx^\mu dx^\nu - dz^2) \quad (3)$$

(and conformal boundary at $z = 0$) is simply cut off at some finite value of the radial coordinate z_0 , whereas in the soft-wall (SW) models a nontrivial dilaton background is used to produce a discrete spectrum with Regge behavior while having $z_0 = \infty$.

Both the top-down and the various bottom-up model eventually describe bulk flavor gauge fields dual to vector and axial vector mesons through a $U(N_f) \times U(N_f)$ Yang-Mills action in a curved five-dimensional background (with or without nontrivial dilaton background),

$$S_{\text{YM}} \propto \text{tr} \int d^4x \int_0^{z_0} dz e^{-\Phi(z)} \sqrt{-g} g^{PR} g^{QS} \left(\mathcal{F}_{PQ}^{(L)} \mathcal{F}_{RS}^{(L)} + \mathcal{F}_{PQ}^{(R)} \mathcal{F}_{RS}^{(R)} \right), \quad (4)$$

where $P, Q, R, S = 0, \dots, 3, z$ and $\mathcal{F}_{MN} = \partial_M \mathcal{B}_N - \partial_N \mathcal{B}_M - i[\mathcal{B}_M, \mathcal{B}_N]$.

In the SS model this action is obtained after truncating the nonpolynomial Dirac-Born-Infeld action and integrating over the four-sphere wrapped by the D8 branes. There g_{MN} is the induced metric on the D8 branes and z_0 is the value of the radial coordinate where the D8 and $\overline{\text{D8}}$ branes connect, which is the extremal value of the geometry for antipodal branes (as we shall assume in what follows). The chiral field $U(x) = \exp[2i\pi(x)/f_\pi]$ appears as the holonomy $U(x) = P \exp i \int \mathcal{B}$ integrated radially along the two connected branes (or, in radial gauge, in the asymptotic behavior of the spatial components of \mathcal{B}). Vector and axial vector fields are even and odd fields over the combined branes, which can be separated into left and right contributions according to $\mathcal{F}_{MN}^{L,R} = \mathcal{F}_{MN}^V \mp \mathcal{F}_{MN}^A$. The physical vector and axial vector mesons correspond to the normalizable modes of these fields. The D8 brane action also involves a Chern-Simons term which leads to the correct Wess-Zumino-Witten term [13, 14]

$$S_{\text{CS}} = \frac{N_c}{24\pi^2} \int \text{tr} \left(\mathcal{B} \mathcal{F}^2 - \frac{i}{2} \mathcal{B}^3 \mathcal{F} - \frac{1}{10} \mathcal{B}^5 \right). \quad (5)$$

(In the bottom-up models, where \mathcal{B}^L and \mathcal{B}^R fields appear separately, this is added by hand as $S_{\text{CS}}^L - S_{\text{CS}}^R$.) The electromagnetic gauge field can be introduced as a non-dynamical background field through a nonzero boundary value for the vector gauge field with generator equal to the electric charge matrix, which naturally leads to vector meson dominance (VMD) [14].

In the following we collect some relevant results for the various models which will then be used to determine the pseudoscalar-photon transition form factors. For more details see Ref. [12] and references therein.

A. Sakai-Sugimoto model

Using a dimensionless coordinate Z that runs from $-\infty$ to $+\infty$ along the connected D8- $\overline{\text{D8}}$ branes, the Yang-Mills part of the action of the SS model reads [13, 14]

$$S_{\text{YM}} = -\kappa \text{Tr} \int d^4x \int_{-\infty}^{\infty} dZ \left[\frac{1}{2} (1 + Z^2)^{-1/3} \eta^{\mu\rho} \eta^{\nu\sigma} \mathcal{F}_{\mu\nu} \mathcal{F}_{\rho\sigma} + (1 + Z^2) M_{\text{KK}}^2 \eta^{\mu\nu} \mathcal{F}_{\mu Z} \mathcal{F}_{\nu Z} \right] \quad (6)$$

with $\kappa = \lambda N_c / (216\pi^3)$ and $\lambda = g_{\text{YM}}^2 N_c$.

Massive vector and axial vector mesons arise as even and odd eigenmodes of $\mathcal{B}_\mu^{(n)} = \psi_n(Z) v_\mu^{(n)}(x)$ with eigenvalue equation

$$-(1 + Z^2)^{1/3} \partial_Z [(1 + Z^2) \partial_Z \psi_n] = \lambda_n \psi_n, \quad \psi_n(\pm\infty) = 0. \quad (7)$$

The lowest mode $v_\mu^{(1)}$ is interpreted as the isotriplet ρ meson (or the ω meson for the U(1) generator) with mass $m_\rho^2 = \lambda_1 M_{\text{KK}}^2$. The numerical result $\lambda_1 = 0.669314\dots$ fixes the Kaluza-Klein mass of the SS model (the inverse radius of the x^4 circle where the D8 and $\overline{\text{D8}}$ branes are localised antipodally) to $M_{\text{KK}} = 949$ MeV.

The holographic factor of the pion wave function is associated to the derivative of the (non-normalizable) zero-mode of (7) of the axial vector sector,

$$\alpha^{\text{SS}}(Z) = \frac{\pi}{2} \arctan(Z). \quad (8)$$

The latter appears in the large gauge transformation that would be needed to enforce a radial gauge $\mathcal{B}_Z = 0$, which relocates the pion field from the holonomy $U(x) = P \exp i \int_{-\infty}^{\infty} dZ \mathcal{B}_Z$ to nontrivial boundary conditions on \mathcal{B}_μ [13]. Either way, the pion decay constant turns out to be given by $f_\pi^2 = \lambda N_c M_{\text{KK}}^2 / (54\pi^4)$. Choosing $f_\pi = 92.4$ MeV corresponds to $\kappa = 0.00745$ or $\lambda \approx 16.63$ for $N_c = 3$.

A background photon field $A_\mu(x)$ is included by setting $\psi(\pm\infty) = 1$ for $\mathcal{B}_\mu = e \mathcal{Q} A_\mu(x) \psi(Z)$ with $\mathcal{Q} = \text{diag}(\frac{2}{3}, -\frac{1}{3}, -\frac{1}{3})$. A real photon with $q^2 = 0$ corresponds to the trivial solution $\psi(Z) \equiv 1$, whereas a virtual photon with spacelike momentum $Q^2 > 0$ is described by solutions where $\lambda_n \rightarrow -Q^2 / M_{\text{KK}}^2$. This defines the so-called bulk-to-boundary propagator, which will be denoted by \mathcal{J} in the following,

$$(1 + Z^2)^{1/3} \partial_Z [(1 + Z^2) \partial_Z \mathcal{J}] = \frac{Q^2}{M_{\text{KK}}^2} \mathcal{J}, \quad \mathcal{J}(Q, Z = \pm\infty) = 1. \quad (9)$$

While the original SS model is a strictly chiral model (and we shall stick to that), masses for quarks can be included through worldsheet instantons [19, 20] which leads to correct GMOR relations. Moreover, at order $1/N_c$ the axial U(1)_A is broken in the SS model, which thereby includes a Witten-Veneziano mechanism [21, 22] for giving mass to the η_0 pseudoscalar according to [13] $m_0^2 = N_f \lambda^2 M_{\text{KK}}^2 / (27\pi^2 N_c)$, which is in the right ballpark to account for realistic pseudoscalar meson masses [23].

However, as mentioned above, the SS model is not asymptotically AdS, but has a diverging dilaton in the UV. It therefore can serve as a dual to QCD only at small momenta.

B. Bottom-up models

1. Hard-wall model with bi-fundamental scalar (HW1)

In the hard-wall model of Ref. [24, 25], a bi-fundamental bulk scalar X is introduced, with a five-dimensional mass term determined by the scaling dimension $\Delta = 3$ of the chiral-symmetry

breaking order parameter $\bar{q}q$ of the boundary theory. At a finite value z_0 , a cutoff of AdS₅ space is imposed with boundary conditions $\mathcal{F}_{z\mu}^{L,R} = 0$.

At zero 4-momentum, the modulus of the scalar field has the form $v(z) = m_q z + \sigma z^3$, where m_q is interpreted as the explicit symmetry-breaking quark mass of the boundary theory, and σ the $\bar{q}q$ condensate. The pion field comes from both the phase of X and the longitudinal components of the axial gauge fields. In the chiral limit, its holographic wave function can be given in closed form as [8, 9]

$$\Psi(z) = \Gamma\left(\frac{2}{3}\right) (\xi z^3/2)^{1/3} \left[I_{-1/3}(\xi z^3) - \frac{I_{2/3}(\xi z_0^3)}{I_{-2/3}(\xi z_0^3)} I_{1/3}(\xi z^3) \right], \quad (10)$$

where $\xi = g_5 \sigma/3$ and $g_5^2 = 12\pi^2/N_c$. The parameter ξ is fixed through the relation

$$\frac{6\pi^2}{N_c} f_\pi^2 = \frac{\Gamma\left(\frac{2}{3}\right)}{\Gamma\left(\frac{4}{3}\right)} \frac{I_{2/3}(\xi z_0^3)}{I_{-2/3}(\xi z_0^3)} (\xi/2)^{2/3}, \quad (11)$$

which yields $\xi = (0.424 \text{ GeV})^3$ for $f_\pi = 92.4 \text{ MeV}$.

Vector mesons have a holographic wave function given by

$$\partial_z \left[\frac{1}{z} \partial_z \psi_n(z) \right] + \frac{1}{z} M_n^2 \psi_n(z) = 0 \quad (12)$$

with boundary conditions $\psi_n(0) = \psi'_n(z_0) = 0$, solved by $\psi_n(z) \propto z J_1(M_n z)$ with M_n determined by the zeros of the Bessel function J_0 . Thereby z_0 gets fixed to $z_0 = \gamma_{0,1}/m_\rho$, where $\gamma_{0,1} = 2.40483\dots$ gives the first zero of J_0 . For $m_\rho = 775 \text{ MeV}$, one obtains $z_0 = 3.103 \text{ GeV}^{-1}$.

The vector bulk-to-boundary propagator is obtained by replacing $M_n^2 \rightarrow -Q^2$ and the boundary conditions by $\mathcal{J}(Q, 0) = 1$ and $\partial_z \mathcal{J}(Q, z_0) = 0$, which gives

$$\mathcal{J}(Q, z) = Qz \left[K_1(Qz) + \frac{K_0(Qz_0)}{I_0(Qz_0)} I_1(Qz) \right]. \quad (13)$$

2. Hirn-Sanz model (HW2)

The hard-wall model by Hirn and Sanz [26] (called HW2 in [12]) refrains from introducing a matrix-valued scalar field for the purpose of chiral symmetry breaking. This is instead implemented in a way that is very similar to the SS model, but in a much simpler manner. The pion field is also built from Wilson lines running along the holographic direction, $U(x) = \xi_R(x) \xi_L(x)$ with $\xi_{L,R} = P \exp(-i \int_0^{z_0} dz \mathcal{B}_z^{L,R})$. Vector and axial vector mesons are distinguished by different boundary conditions on the hard wall, Neumann for vector and Dirichlet for axial vector mesons, which is precisely what distinguishes them in the SS model at the point where D8 and $\bar{D}8$ branes connect. As in the SS model, the pion wave function appears as the derivative of a non-normalizable zero mode α of the axial vector field,

$$\alpha^{\text{HW2}}(z) = 1 - \frac{z^2}{z_0^2}. \quad (14)$$

The vector meson field equation is the same as in the HW1 model, and therefore also the vector bulk-to-boundary propagator \mathcal{J} , Eq. (13), as well as the value of z_0 .

3. Soft-wall model

Soft-wall models were originally introduced to achieve a Regge-type spectrum of mesons [27]. Prescribing by hand a nontrivial background dilaton field $\Phi(z) = \kappa^2 z^2$ leads to $M_n^2 = 4\kappa^2(n+1)$ for the vector mesons, where $\kappa = m_\rho/2$. Since now $z_0 = \infty$, the boundary conditions in the IR are replaced by the requirement of normalizability.

The vector field equation is given by (12) with $1/z$ replaced by $e^{-\kappa^2 z^2}/z$. A closed form solution for \mathcal{J} can be given in terms the confluent hypergeometric function of the second kind $U(a, b, z)$:

$$\mathcal{J}^{\text{SW}}(Q, \kappa, z) = \frac{U(\frac{Q^2}{4\kappa^2}, 0, (\kappa z)^2)}{U(\frac{Q^2}{4\kappa^2}, 0, 0)} = \Gamma(1 + \frac{Q^2}{4\kappa^2})U(\frac{Q^2}{4\kappa^2}, 0, (\kappa z)^2). \quad (15)$$

In this model chiral symmetry breaking is implemented in a less clear manner. The soft-wall model considered in [12] (and also here) follows Ref. [28], where the pion wave function is assumed to be Gaussian,

$$\alpha^{\text{SW}}(z) = e^{-\kappa^2 z^2}. \quad (16)$$

III. PSEUDOSCALAR-PHOTON TRANSITION FORM FACTORS

The pseudoscalar-photon TFF is defined by

$$\int d^4x e^{-iq_1 \cdot x} \langle P(q_1 + q_2) | T \{ J_\mu^{e.m.}(x) J_\nu^{e.m.}(0) \} | 0 \rangle = \epsilon_{\mu\nu\rho\sigma} q_1^\rho q_2^\sigma F_{P\gamma^*\gamma^*}(Q_1^2, Q_2^2), \quad (17)$$

where $Q_{1,2}^2 = -q_{1,2}^2$. For $P = \pi^0$ the value for real photons is determined by the axial anomaly according to

$$F_{\pi^0\gamma^*\gamma^*}(0, 0) = \frac{N_c}{12\pi^2 f_\pi}. \quad (18)$$

A. Holographic predictions

In the following we shall denote the normalized TFF by K ,

$$K(Q_1^2, Q_2^2) \equiv F(Q_1^2, Q_2^2)/F(0, 0), \quad (19)$$

and consider the various holographic predictions in the chiral limit. The derivation of the holographic result has been discussed in detail in Refs. [9, 10, 12, 29] for the various models, in Ref. [11] also by including the effects of finite quark masses in the HW1 model. It is determined by the universal form of the Chern-Simons action needed to take into account the chiral anomaly, which leads to an integral over two bulk-to-boundary propagators for the virtual photons times the holographic pion wave function,

$$K(Q_1^2, Q_2^2) = - \int_0^{z_0} \mathcal{J}(Q_1, z) \mathcal{J}(Q_2, z) \partial_z \alpha(z) dz. \quad (20)$$

In the case of the HW1 model, this needs to be corrected by a boundary term in the infrared [9], because the HW1 pion wave function $\Psi(z_0) \neq 0$,

$$K^{\text{HW1}}(Q_1^2, Q_2^2) = - \int_0^{z_0} \mathcal{J}(Q_1, z) \mathcal{J}(Q_2, z) \partial_z \Psi(z) dz + \mathcal{J}(Q_1, z_0) \mathcal{J}(Q_2, z_0) \Psi(z_0). \quad (21)$$

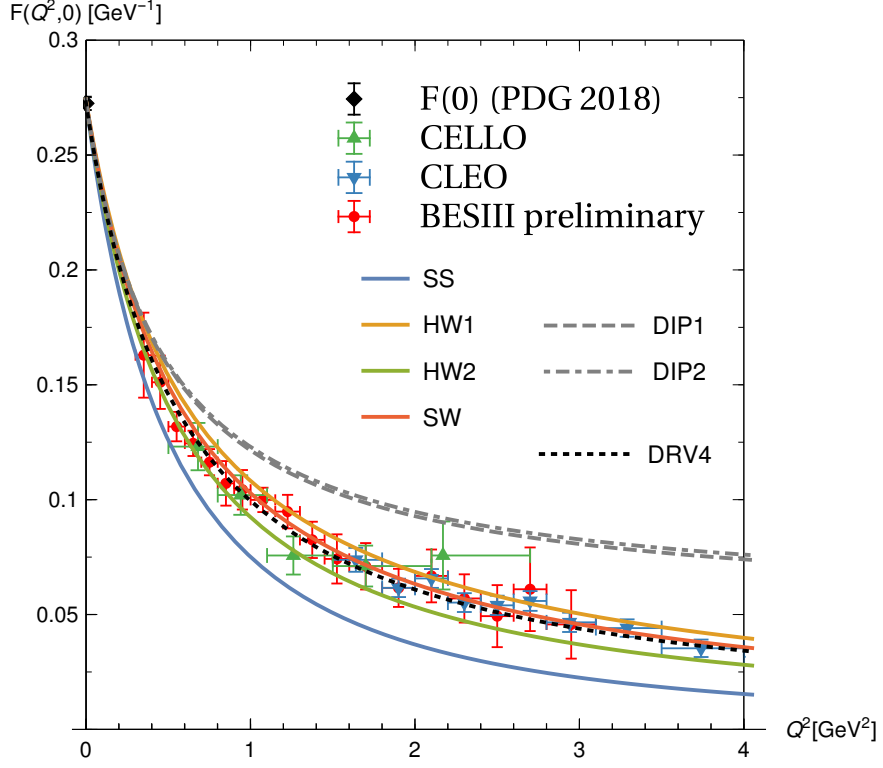


FIG. 1. Data for the π^0 TTF from CELLO, CLEO, BESIII-preliminary as compiled in Fig. 3 of Ref. [7] compared to the results of the various holographic models, the interpolators (DIP1, DIP2) proposed in Ref. [12] with curvature parameter $\hat{\beta}$ matched to the bottom-up holographic models, and the recent improved interpolator of Ref. [7] fitting the experimental data up to 4 GeV (DRV4). (The fit up to 9 GeV used in the evaluation of a_μ happens to agree so closely with the SW prediction that it could not be distinguished within the line thickness of this plot.)

B. Low- Q^2 behavior and comparison to data

The behavior of $K(Q_1^2, Q_2^2)$ at virtualities below 1 GeV^2 are decisive for the HLBL contribution to a_μ . It is therefore of interest to parametrize the low- Q^2 behavior by the first few Taylor coefficients, which following [12] we define by

$$K(Q_1^2, Q_2^2) = 1 + \hat{\alpha}(Q_1^2 + Q_2^2) + \hat{\beta}Q_1^2Q_2^2 + \hat{\gamma}(Q_1^4 + Q_2^4) + O(Q^6). \quad (22)$$

The slope parameter $\hat{\alpha}$ is often quoted as $a_\pi = -\hat{\alpha}m_\pi^2$ or $\Lambda^2 = -1/\hat{\alpha}$.

In Table I, these parameters are given for the various holographic models. Until recently, the experimental world average for $\hat{\alpha}$, which was dominated by the result of the CELLO collaboration [6], read $\hat{\alpha} = -1.76(22) \text{ GeV}^{-2}$. In Ref. [12] this was taken as an indication that the SS model, which has $\hat{\alpha}^{\text{SS}} = -2.043$, should be discarded as a viable model for the pion TFF. A recent analysis of Dalitz decays of π^0 from NA62 gave [30] $\hat{\alpha} = -2.02(31) \text{ GeV}^{-2}$, leading to the new world average [2] $-1.84(17) \text{ GeV}^{-2}$. The previous world average and its error had covered all results of the bottom-up models, while being at some tension with the SS model, but now also the HW1 model is slightly disfavored, while optimal agreement is found for the HW2 model.

In Fig. 1, the holographic results are compared with spacelike π^0 TFF data at $Q^2 \leq 4 \text{ GeV}^2$ as compiled in Fig. 3 of Ref. [7], which includes preliminary data from BESIII down to 0.3 GeV^2 . At the lowest available Q^2 value, all holographic results are within the experimental error bar, while

Model	$\Lambda^2[\text{GeV}^2]$	$\hat{\alpha}[\text{GeV}^{-2}]$	$\hat{\beta}[\text{GeV}^{-4}]$	$\hat{\gamma}[\text{GeV}^{-4}]$	$\bar{F}(0, \infty)$	$\bar{F}(\infty, \infty)$
SS	0.489	-2.043	4.56	3.55	0	0
HW1	0.627	-1.595	3.01	2.63	1.00	1.00
HW2	0.554	-1.805	3.65	3.06	0.62	0.62
SW	0.601	-1.665	3.56	2.76	0.89	0.89
DIP1	0.568	-1.760	3.33	3.78	∞	1.00
DIP2	0.568	-1.760	3.33	3.88	∞	1.00
DRV4	0.574	-1.742	∞	3.04	0.85	0.85
DRV9	0.611	-1.637	∞	2.68	0.90	0.90

TABLE I. IR and UV behavior of $K(Q_1^2, Q_2^2)$ in the top-down holographic SS model and the three bottom-up models HW1, HW2, and SW considered here (all in the chiral limit), with IR coefficients as defined in (22) and $\Lambda^2 \equiv -1/\hat{\alpha}$; the UV behavior is described by $\bar{F} = F/F^\infty$, where F^∞ is the LO QCD result (25). Also given are the corresponding quantities of the interpolators (31) and (32) (DIP1 and DIP2) used in [12] to approximate the bottom-up models with respect to $\hat{\alpha}$ and $\hat{\beta}$, and the DRV interpolator (30) used in [7] to fit the currently available data up to 4 or 9 GeV².

at higher Q^2 the SS model underestimates the experimental result. All the bottom-up holographic results are however found to agree remarkably well with the data. As we shall discuss next, this correlates with their behavior at very high Q^2 .

C. Short-distance behavior

Perturbative QCD predicts a factorization of the double virtual TFF into a perturbatively calculable hard-scattering kernel and a nonperturbative meson distribution amplitude [16, 31]. To leading order (LO), an asymptotic pion distribution function $\Phi_\pi(x) = 6x(1-x)$, where x and $(1-x)$ are the momentum fractions of a collinear quark/anti-quark state, yields [7]

$$K^\infty(Q_1^2, Q_2^2) = \frac{8\pi^2 f_\pi^2}{Q_1^2 + Q_2^2} f(w) \quad (23)$$

with $w = (Q_1^2 - Q_2^2)/(Q_1^2 + Q_2^2)$ and

$$f(w) = \frac{1}{w^2} - \frac{1-w^2}{2w^3} \ln \frac{1+w}{1-w}, \quad (24)$$

which equals unity at $w = \pm 1$ and drops to $f(0) = 2/3$ at the symmetric point. This corresponds to asymptotic behavior

$$F^\infty(Q^2, 0) = \frac{2f_\pi}{Q^2}, \quad F^\infty(Q^2, Q^2) = \frac{2f_\pi}{3Q^2}. \quad (25)$$

Perturbative corrections have been worked out in Ref. [32] to order α_s and α_s^2 ; they lead to a moderate reduction of the LO result for $Q^2 \gtrsim 2 \text{ GeV}^2$, but evidently much higher values of Q^2 are needed for the experimental data to approach the perturbative regime.

As shown in [9], the HW1 model has an asymptotic limit equal to the full LO pQCD result, when the parameter σ is fixed according to (11). Amazingly, exactly the same w -dependence arises

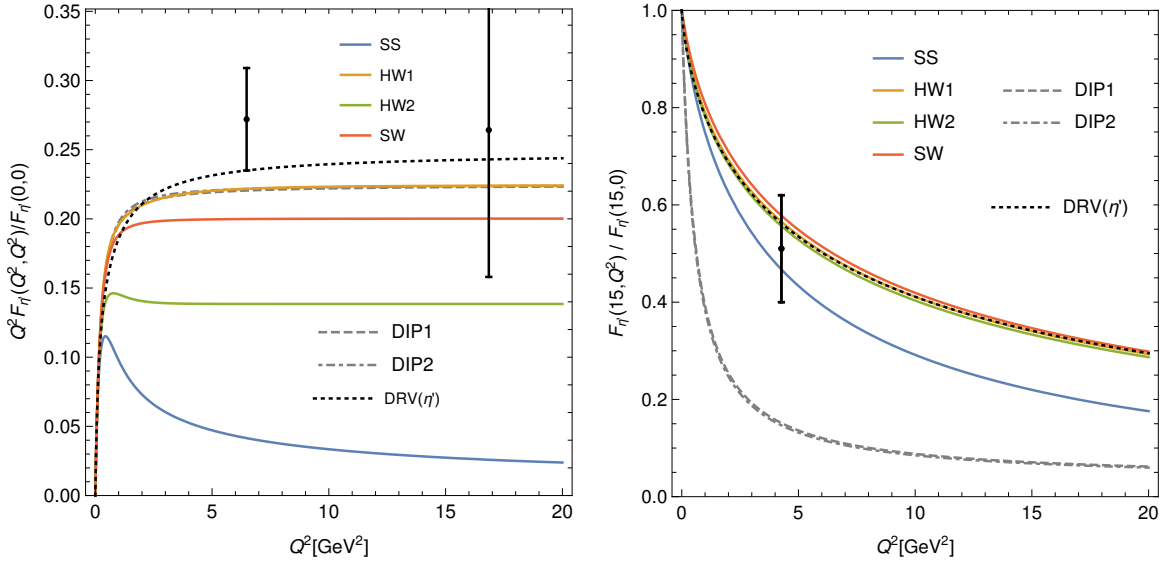


FIG. 2. Comparison of the results for symmetric and asymmetric double-virtual TFF with experimental data for η' from BaBar [33]. For the holographic models and the DIP1,2 interpolators the results of the chiral limit have been simply rescaled by the experimental value for $f_\pi/f_{\eta'}$, while $\text{DRV}(\eta')$ is determined by a fit to experimental data for $F_{\eta'}(Q^2, 0)$.

for $Q^2 \rightarrow \infty$:

$$\begin{aligned} K^{\text{HW1}}(Q_1^2, Q_2^2) &\rightarrow \frac{8\pi^2 f_\pi^2}{Q_1^2 + Q_2^2} \sqrt{1-w^2} \int_0^\infty d\xi \xi^3 K_1(\xi\sqrt{1+w}) K_1(\xi\sqrt{1-w}) \\ &= \frac{8\pi^2 f_\pi^2}{Q_1^2 + Q_2^2} f(w), \end{aligned} \quad (26)$$

where $\xi = Qz$ and $f(w)$ as given in (24).

Apart from a different overall factor, the same form is found in the other bottom-up models, which is a direct consequence of the asymptotic AdS geometry [12].

In the HW2 model, the factor $8\pi^2 f_\pi^2$ is replaced by $4/z_0^2$. With $z_0 = 3.103 \text{ GeV}^{-1}$ in order to reproduce the value of the ρ meson mass, this corresponds to $\approx 61.6\%$ of the LO pQCD result.

In the SW model, the prefactor is instead $4\kappa^2$, with the same integral resulting in the limit $Q^2 \gg \kappa^2$ because

$$\mathcal{J}^{\text{SW}}(Q, \kappa, z) = \frac{U(\frac{Q^2}{4\kappa^2}, 0, (\kappa z)^2)}{U(\frac{Q^2}{4\kappa^2}, 0, 0)} \rightarrow (Qz) K_1(Qz) \quad (27)$$

and the extra factor $e^{-\kappa^2 \xi^2 / Q^2}$ in the pion wave function becoming negligible. With $\kappa = m_\rho/2$, the overall factor is thus reduced to $m_\rho^2 / (8\pi^2 f_\pi^2) \approx 0.893$.

The top-down holographic QCD model of Sakai and Sugimoto on the other hand is only meaningful in the low-energy limit. Here the asymptotic geometry is not AdS_5 but instead six-dimensional with a diverging dilaton. Considering nevertheless the limit $Q/M_{\text{KK}} \rightarrow \infty$, we find

$$\mathcal{J}^{\text{SS}}(Q, \zeta) \rightarrow \left(1 + 3\bar{Q}\zeta^{\frac{1}{3}}\right) e^{-3\bar{Q}\zeta^{\frac{1}{3}}} \quad (28)$$

with $\bar{Q} = Q/M_{\text{KK}}$ and thus

$$K^{\text{SS}}(Q_1^2, Q_2^2) \rightarrow \frac{16}{9\pi} \left(\frac{2M_{\text{KK}}^2}{Q_1^2 + Q_2^2} \right)^{\frac{3}{2}} \frac{2 + 5\sqrt{1-w^2}}{(\sqrt{1-w} + \sqrt{1+w})^5}. \quad (29)$$

This different w -dependence turns out to be rather similar quantitatively to that of the bottom-up models: At constant $Q_1^2 + Q_2^2$, the ratio of symmetrically double-virtual $K(Q^2/2, Q^2/2)$ over single-virtual $K(Q^2, 0)$, which at LO pQCD equals $2/3$, asymptotes to $7/(8\sqrt{2}) \approx 0.62$ in the SS model. The more significant difference is in the faster falloff $\sim Q^{-3}$, which highlights the fact that the SS model is applicable only in the low- Q^2 regime.

In Table I the short-distance behavior of the various models is listed in comparison to the LO pQCD result, defining $\bar{F}(Q_1^2, Q_2^2) = F(Q_1^2, Q_2^2)/F^\infty(Q_1^2, Q_2^2)$. The DIP interpolators (defined below in (31) and (32)) reproduce by construction the correct limit for $Q_1^2 = Q_2^2 \rightarrow \infty$, but cannot satisfy the Brodsky-Lepage constraint [16] of nontrivial asymptotic Q^{-2} behavior in the single virtual case. The DRV interpolator that was recently proposed in [7] is defined by

$$K^{\text{DRV}}(Q_1^2, Q_2^2) = \frac{1}{1 + (Q_1^2 + Q_2^2)/\Lambda^2} f(w_\Lambda),$$

$$w_\Lambda \equiv \left(\frac{(Q_1^2 - Q_2^2)^2 + \Lambda^4}{(Q_1^2 + Q_2^2)^2 + \Lambda^4} \right)^{1/2}. \quad (30)$$

It has by construction an asymptotic $Q^{-2}f(w)$ behavior, without being fixed to the LO pQCD prefactor. The overall factor instead depends on the value of the single fitting parameter Λ and is given in Table I for the two fits of the pion TFF data presented in [7]. Notice that the DRV interpolator has a logarithmically divergent curvature in the double-virtual case as $Q_{1,2}^2 \rightarrow 0$.

In [7] the DRV interpolator has been compared with recent experimental data from BaBar [33] for double virtual $F_{\eta'}(Q_1^2, Q_2^2)$. In Fig. 2 this comparison is extended to the holographic models and the DIP interpolators. The bottom-up models with the largest UV prefactor, the HW1 and SW models, compare favorably with the data for symmetric double virtual TFF, while the HW2 is further away, and the SS model clearly completely off. However, it should be kept in mind that for the application to a_μ only comparatively small values of Q^2 will be relevant. In Fig. 2 also the asymmetric double virtual TFF for η' is considered, with one data point from BaBar [33]. Interestingly enough, the SS result for the ratio $F_{\eta'}(15, Q_2^2)/F_{\eta'}(15, 0)$ is not too far from the pQCD result, which at these momenta are closely reproduced by the bottom-up models and the DRV interpolator, and all agree with the experimental value within errors, whereas the DIP ansatz fails to reproduce it.

Unfortunately, there are not yet experimental data for the double-virtual pion TFF for low values of Q^2 , but these could be provided by BESIII around and below 1 GeV^2 in the future [7]. However, there exists a new lattice QCD calculation [15], which extrapolates its results to arbitrary Q_1^2 and Q_2^2 . This is compared with the holographic results and the DIP1,2 and DRV4 interpolators in Fig. 3. In the symmetrically double-virtual case, the lattice result for $Q^2 F(Q^2, Q^2)/F(0, 0)$ is in between the bottom-up holographic results, with the SW model almost coinciding with the lattice result, whereas the DRV interpolator takes much longer to flatten out. The SS model result drops already above 0.5 GeV^2 , where its incorrect short-distance behavior starts to dominate. Also shown are the various predictions for the dependence on x of the asymmetric double-virtual TFF $F((1-x)\text{GeV}^2, x\text{GeV}^2)/F(0, 0)$ at fixed $Q_1^2 + Q_2^2$, where all holographic results have a much milder dependence on x than the DRV interpolator, with the lattice result of [15] being closer to the former.

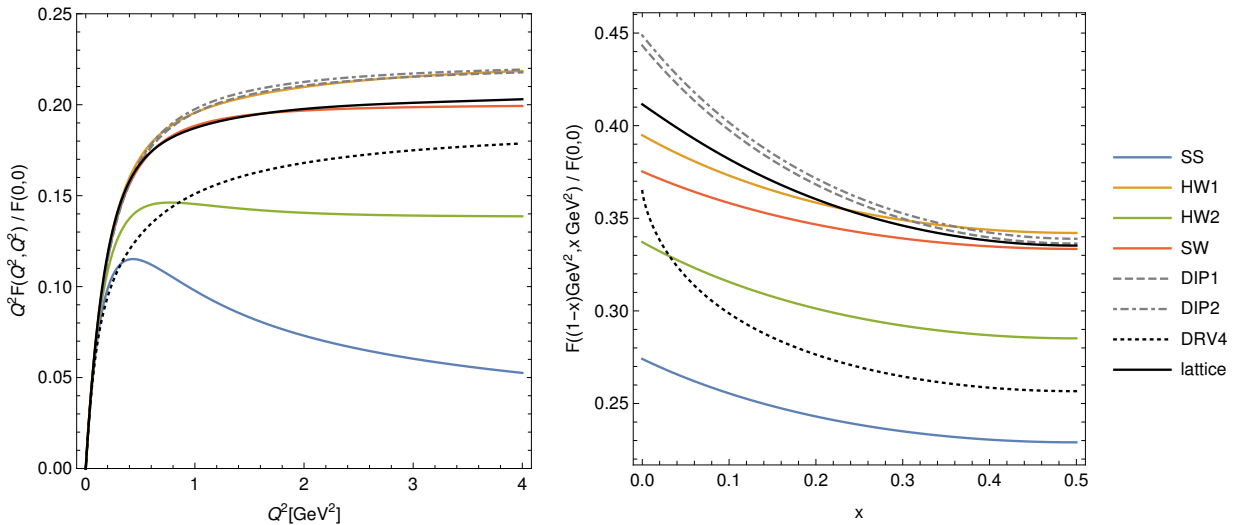


FIG. 3. Comparison of the predictions for the symmetrically double-virtual pion TFF $Q^2 F(Q^2, Q^2)/F(0,0)$ (left plot) and for the dependence on x in the asymmetric $F((1-x)\text{GeV}^2, x\text{GeV}^2)/F(0,0)$, i.e., at $Q_1^2 + Q_2^2 = 1\text{GeV}^2$, (right plot) including the recent lattice extrapolations of Ref. [15] (corresponding to the central line of Fig. 7 therein).

IV. HADRONIC LIGHT-BY-LIGHT CONTRIBUTION TO THE MUON $g - 2$

In order to use the holographic QCD results for the HLBL contribution to a_μ without having to use the full 3-dimensional integral representation of the relevant two-loop diagram, Ref. [12] employed two variants of (extended) DIP interpolators,

$$K(Q_1^2, Q_2^2)^{\text{DIP1}} = 1 + \lambda \left(\frac{Q_1^2}{Q_1^2 + m_1^2} + \frac{Q_2^2}{Q_2^2 + m_2^2} \right) + \sum_{i=1}^2 \eta_i \frac{Q_1^2 Q_2^2}{(Q_1^2 + m_i^2)(Q_2^2 + m_i^2)} \quad (31)$$

$$K(Q_1^2, Q_2^2)^{\text{DIP2}} = 1 + \sum_{i=1}^2 \lambda_i \left(\frac{Q_1^2}{Q_1^2 + m_i^2} + \frac{Q_2^2}{Q_2^2 + m_i^2} \right) + \eta \frac{Q_1^2 Q_2^2}{(Q_1^2 + m_1^2)(Q_2^2 + m_1^2)}, \quad (32)$$

where $m_2 = m_\rho$ and the free parameters were used to include a slope parameter $\hat{\alpha} = -1.76$ in accordance with the current world average and also the range obtained by the bottom-up models. Only one of the curvature parameters could be matched at a time and preference was given to the parametrization obtained by fitting $\hat{\beta}$ to the average value of 3.33GeV^{-4} . Finally, the remaining parameter was fixed by requiring agreement with the LO QCD result F^∞ at $Q_1^2 = Q_2^2 \rightarrow \infty$. The Brodsky-Lepage constraint [16] could however not be incorporated simultaneously. The finite limit $K^{\text{DIP1,2}}(Q^2 \rightarrow \infty, 0)$ was instead taken as representing a nonzero value of the magnetic susceptibility χ_0 appearing in the short-distance behavior far away from the pion pole [34], $F_{\pi^0 * \gamma^* \gamma^*}(Q^2 \rightarrow \infty, Q^2 \rightarrow \infty, 0) \rightarrow -f_\pi \chi_0 / 3$. The latter would be of interest in evaluations beyond the pion-pole approximation considered here (in particular with the HW1 model, which has a nonvanishing χ_0 [35]).

In Table II we show the results of the full 3-dimensional integration that we have carried out using the formulae of Ref. [5] with the holographic results for $K(Q_1^2, Q_2^2)$ (which also require numerical evaluation). The estimated numerical error of our results is below $1 \cdot 10^{-12}$. In Fig. 4 we also display the error of the integrations when these are cut off at some value Q^{max} for both loop momenta, showing the slightly different convergence behavior of the various models. Evidently,

Model	$a_\mu^{\pi^0}$	a_μ^η	$a_\mu^{\eta'}$	sum
SS	4.83	1.17	0.78	6.77
HW1	6.13	1.67	1.20	8.99
HW2	5.66	1.48	1.03	8.17
SW	5.92	1.59	1.12	8.63
DIP1	6.54	1.90	1.44	9.89
DIP2	6.58	1.92	1.46	9.97
DRV [7]	5.6(2)	1.5(1)	1.3(1)	8.4(4)

TABLE II. Results in multiples of 10^{-10} for $f_\pi = 92.4$ MeV for the Sakai-Sugimoto model, three bottom-up models, and the DIP interpolation of Ref. [12] based on the curvature $\hat{\beta}$ averaged over the bottom-up models. The last line refers to the new interpolator (DRV) of Ref. [7] fitted to experimental data including the preliminary ones from BESIII. Numerical errors in the integrations carried out for the holographic models are estimated as smaller than $1 \cdot 10^{-12}$. For estimating also the contributions a_μ^η and $a_\mu^{\eta'}$ we have included the experimental masses for η and η' , but kept the results for $K(Q_1^2, Q_2^2)$ obtained in the chiral limit and simply rescaled $F(0, 0)$ by the central experimental values quoted in [7]. The holographic results do not include the experimental errors for the various $F(0, 0)$, which in a_μ amount to about $\pm 2\%$, 3.5% , and 4.5% for π^0 , η , and η' , respectively.

the DIP interpolators do not well represent the results of the bottom-up models but overestimate them by an amount which is larger than their deviations from each other. This is in line with the discrepancy displayed in Figs. 1 and 2 between the TFF of the bottom-up models and the DIP interpolators.

Given that the bottom-up holographic models are all in remarkable agreement with the low-energy data for single-virtual pion TFF as shown in Fig. 1, while also bracketing the lattice results [15] of double-virtual TFF (Fig. 3), they provide, taken together, an arguably strong prediction for a_μ consisting of the range $(5.7 \dots 6.1) \cdot 10^{-10} = 5.9(2) \cdot 10^{-10}$. [Notice that this does not include the experimental uncertainty in $F_{\pi^0}(0, 0)$, but corresponds to the choice $f_\pi = 92.4$ MeV in (18).]

In Table II these results are also compared with the result obtained in Ref. [7] with a new interpolator (DRV), fitted to experimental data up to 9 GeV² for π^0 including the preliminary ones from BESIII. This fit for single-virtual pion TFF happens to be indistinguishable from the SW model within the line thickness in Fig. 1, but for double-virtual TFF there are significant differences as shown in Fig. 3. In fact, the SW model yields a somewhat higher value than obtained by the DRV interpolator.

Also given are extrapolations to a_μ^η and $a_\mu^{\eta'}$ using the same function K but rescaling $F(0, 0)$ according to the central experimental values quoted in [7] ($F_\eta(0, 0)/F_{\pi^0}(0, 0) = 0.2736/0.2725$ and $F_{\eta'}(0, 0)/F_{\pi^0}(0, 0) = 0.3412/0.2725$).¹

V. CONCLUSION AND OUTLOOK

As displayed in Fig. 1, the bottom-up AdS/QCD models considered here and previously in Ref. [12] reproduce remarkably well the available experimental data for the single-virtual pion TFF, including the preliminary data from BESIII presented recently in Ref. [7]. The top-down model of Sakai and Sugimoto turns out to have a larger slope parameter but also larger upward

¹ An approximate evaluation of $a_\mu^{\pi^0, \eta, \eta'}$ has been carried out for the HW1 model including finite quark masses in Ref. [11], but using only a finite number of vector meson modes. The results given in Ref. [11] are significantly higher than ours in the chiral limit, even for $a_\mu^{\pi^0}$, although the full single-virtual pion TFF obtained there seems to be extremely close to our result.

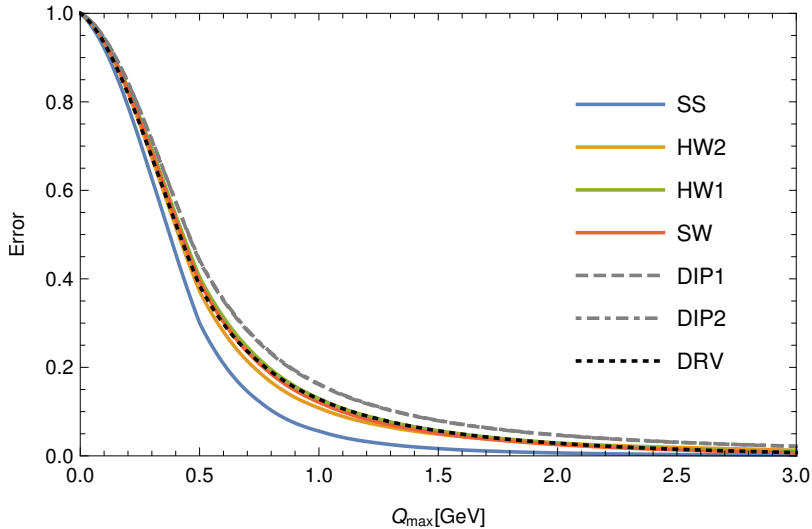


FIG. 4. Remaining errors in the integral for $a_\mu^{\pi^0}$, when this is cut off at $Q_1^{\max} = Q_2^{\max} = Q_{\max}$ (plotted over Q_{\max} instead of Q_{\max}^2 to spread out the low- Q region).

curvature compared to the bottom-up models. At the smallest values of Q^2 this seems perfectly consistent with the preliminary data from BESIII, but for all $Q^2 > 0.5 \text{ GeV}^2$ the experimental data are underestimated, so that the result for $a_\mu^{\pi^0, \text{SS}}$ of $4.8 \cdot 10^{-10}$ could perhaps be taken as a lower limit to which positive contributions necessary to make contact with the correct short-distance behavior need to be added.² The bottom-up holographic models, on the other hand, reproduce the asymptotic pQCD behavior either perfectly or to a large percentage, as shown in Table I.

The DIP interpolators used in Ref. [12] to approximate the bottom-up models appear to overestimate all the results for the pion TFF both with respect to the holographic models as well as the experimental data. Moreover, they fail to include the Brodsky-Lepage constraint [16]. From the full evaluation of the pion-pole contribution to a_μ in the holographic models as carried out here, we arrive at somewhat smaller numbers than presented in Ref. [12]: instead of the value $a_\mu^{\pi^0} = 6.54(25) \cdot 10^{-10}$, quoted therein, we find that the spread of the bottom-up AdS/QCD results is given by $5.9(2) \cdot 10^{-10}$ for fixed $f_\pi = 92.4 \text{ MeV}$. This is in between the central results given by a simple VMD model ($a_\mu^{\text{VMD}} = 5.7 \cdot 10^{-10}$) and the LMD+V model ($a_\mu^{\text{VMD}} = 6.3 \cdot 10^{-10}$) [5], it is at the lower end of the result [36] ($a_\mu^{\text{dispersive}} = 6.3(3) \cdot 10^{-10}$) obtained in the dispersion theory framework of Ref. [37], but it happens to agree remarkably well with the recent lattice result [15] of $5.97(36) \cdot 10^{-10}$ for the pion-pole contribution. The bottom-up holographic results are somewhat higher than the result $5.6(2) \cdot 10^{-10}$ obtained with the new (DRV) interpolator introduced in Ref. [7], which has a stronger dependence on the asymmetry parameter w (defined in (24)) than both the holographic and the lattice results. It will be interesting to see how these results for the double-virtual pion TFF compare with future improvements of low-energy experimental or lattice data.

Since the central value $5.9 \cdot 10^{-10}$ of the holographic results for $a_\mu^{\pi^0}$ is given by the SW model, which for the single-virtual pion TFF practically coincides with the DRV9 interpolator used in Ref. [7] to account for the new experimental data, while agreeing much better with the currently best lattice results for the double-virtual pion TFF of Ref. [15], this result could already be taken

² In future work we plan to consider also glueball-photon couplings as obtained in the SS model [to appear] and the resulting HLBL contribution to a_μ . The present analysis suggests that the latter would be underestimated by some 20% due to the incorrect UV behavior of the SS model, which is perhaps not too bad in view of the wider uncertainties of such calculations.

as an improvement of the estimate of [7], increasing the latter by $0.3 \cdot 10^{-10}$.

ACKNOWLEDGMENTS

We thank Massimiliano Procura for most useful discussions as well as Luigi Cappiello, Oscar Catà, Giancarlo D’Ambrosio, Deog Ki Hong, and Doyoun Kim for correspondence. We are particularly grateful to Igor Danilkin for providing checks of our numerical calculations. J. L. was supported by the FWF doctoral program Particles & Interactions, project no. W1252-N27.

-
- [1] F. Jegerlehner and A. Nyffeler, *The Muon $g - 2$* , *Phys. Rept.* **477** (2009) 1–110, [[arXiv:0902.3360](#)].
 - [2] M. Tanabashi et al., *Review of Particle Physics*, *Phys. Rev. D* **98** (2018) 030001.
 - [3] A. Keshavarzi, D. Nomura, and T. Teubner, *Muon $g - 2$ and $\alpha(M_Z^2)$: a new data-based analysis*, *Phys. Rev.* **D97** (2018) 114025, [[arXiv:1802.02995](#)].
 - [4] M. Knecht and A. Nyffeler, *Hadronic light by light corrections to the muon $g - 2$: The Pion pole contribution*, *Phys. Rev.* **D65** (2002) 073034, [[hep-ph/0111058](#)].
 - [5] A. Nyffeler, *Precision of a data-driven estimate of hadronic light-by-light scattering in the muon $g - 2$: Pseudoscalar-pole contribution*, *Phys. Rev.* **D94** (2016) 053006, [[arXiv:1602.03398](#)].
 - [6] **CELLO** Collaboration, H. J. Behrend et al., *A Measurement of the π^0 , η and η' electromagnetic form-factors*, *Z. Phys.* **C49** (1991) 401–410.
 - [7] I. Danilkin, C. F. Redmer, and M. Vanderhaeghen, *The hadronic light-by-light contribution to the muon’s anomalous magnetic moment*, *Prog. Part. Nucl. Phys.* **107** (2019) 20–68, [[arXiv:1901.10346](#)].
 - [8] H. R. Grigoryan and A. V. Radyushkin, *Pion form-factor in chiral limit of hard-wall AdS/QCD model*, *Phys. Rev.* **D76** (2007) 115007, [[arXiv:0709.0500](#)].
 - [9] H. R. Grigoryan and A. V. Radyushkin, *Anomalous Form Factor of the Neutral Pion in Extended AdS/QCD Model with Chern-Simons Term*, *Phys. Rev.* **D77** (2008) 115024, [[arXiv:0803.1143](#)].
 - [10] H. R. Grigoryan and A. V. Radyushkin, *Pion in the Holographic Model with 5D Yang-Mills Fields*, *Phys. Rev.* **D78** (2008) 115008, [[arXiv:0808.1243](#)].
 - [11] D. K. Hong and D. Kim, *Pseudo scalar contributions to light-by-light correction of muon $g - 2$ in AdS/QCD*, *Phys. Lett.* **B680** (2009) 480–484, [[arXiv:0904.4042](#)].
 - [12] L. Cappiello, O. Cata, and G. D’Ambrosio, *The hadronic light by light contribution to the $(g - 2)_\mu$ with holographic models of QCD*, *Phys. Rev.* **D83** (2011) 093006, [[arXiv:1009.1161](#)].
 - [13] T. Sakai and S. Sugimoto, *Low energy hadron physics in holographic QCD*, *Prog.Theor.Phys.* **113** (2005) 843–882, [[hep-th/0412141](#)].
 - [14] T. Sakai and S. Sugimoto, *More on a holographic dual of QCD*, *Prog.Theor.Phys.* **114** (2005) 1083–1118, [[hep-th/0507073](#)].
 - [15] A. Gérardin, H. B. Meyer, and A. Nyffeler, *Lattice calculation of the pion transition form factor with $N_f = 2 + 1$ Wilson quarks*, [arXiv:1903.09471](#).
 - [16] G. P. Lepage and S. J. Brodsky, *Exclusive Processes in Quantum Chromodynamics: Evolution Equations for Hadronic Wave Functions and the Form-Factors of Mesons*, *Phys. Lett.* **87B** (1979) 359–365.
G. P. Lepage and S. J. Brodsky, *Exclusive Processes in Perturbative Quantum Chromodynamics*, *Phys. Rev.* **D22** (1980) 2157.
S. J. Brodsky and G. P. Lepage, *Large Angle Two Photon Exclusive Channels in Quantum Chromodynamics*, *Phys. Rev.* **D24** (1981) 1808.
 - [17] J. M. Maldacena, *The Large N limit of superconformal field theories and supergravity*, *Int.J.Theor.Phys.* **38** (1999) 1113–1133, [[hep-th/9711200](#)].
 - [18] E. Witten, *Anti-de Sitter space, thermal phase transition, and confinement in gauge theories*, *Adv.Theor.Math.Phys.* **2** (1998) 505–532, [[hep-th/9803131](#)].
 - [19] O. Aharony and D. Kutasov, *Holographic Duals of Long Open Strings*, *Phys.Rev.* **D78** (2008) 026005, [[arXiv:0803.3547](#)].

- [20] K. Hashimoto, T. Hirayama, F.-L. Lin, and H.-U. Yee, *Quark Mass Deformation of Holographic Massless QCD*, *JHEP* **0807** (2008) 089, [[arXiv:0803.4192](#)].
- [21] E. Witten, *Current Algebra Theorems for the U(1) “Goldstone Boson”*, *Nucl.Phys.* **B156** (1979) 269.
- [22] G. Veneziano, *U(1) Without Instantons*, *Nucl.Phys.* **B159** (1979) 213–224.
- [23] F. Brünner and A. Rebhan, *Constraints on the $\eta\eta'$ decay rate of a scalar glueball from gauge/gravity duality*, *Phys. Rev.* **D92** (2015) 121902, [[arXiv:1510.07605](#)].
- [24] J. Erlich, E. Katz, D. T. Son, and M. A. Stephanov, *QCD and a holographic model of hadrons*, *Phys. Rev. Lett.* **95** (2005) 261602, [[hep-ph/0501128](#)].
- [25] L. Da Rold and A. Pomarol, *Chiral symmetry breaking from five dimensional spaces*, *Nucl. Phys.* **B721** (2005) 79–97, [[hep-ph/0501218](#)].
- [26] J. Hirn and V. Sanz, *Interpolating between low and high energy QCD via a 5-D Yang-Mills model*, *JHEP* **12** (2005) 030, [[hep-ph/0507049](#)].
- [27] A. Karch, E. Katz, D. T. Son, and M. A. Stephanov, *Linear confinement and AdS/QCD*, *Phys. Rev.* **D74** (2006) 015005, [[hep-ph/0602229](#)].
- [28] H. R. Grigoryan and A. V. Radyushkin, *Structure of vector mesons in holographic model with linear confinement*, *Phys. Rev.* **D76** (2007) 095007, [[arXiv:0706.1543](#)].
- [29] A. Stoffers and I. Zahed, *$\gamma^*\gamma^* \rightarrow \pi^0$ Form Factor from AdS/QCD*, *Phys. Rev.* **C84** (2011) 025202, [[arXiv:1104.2081](#)].
- [30] **NA62** Collaboration, C. Lazzeroni et al., *Measurement of the π^0 electromagnetic transition form factor slope*, *Phys. Lett.* **B768** (2017) 38–45, [[arXiv:1612.08162](#)].
- [31] A. V. Efremov and A. V. Radyushkin, *Factorization and Asymptotical Behavior of Pion Form-Factor in QCD*, *Phys. Lett.* **94B** (1980) 245–250.
- [32] B. Melic, D. Mueller, and K. Passek-Kumericki, *Next-to-next-to-leading prediction for the photon to pion transition form-factor*, *Phys. Rev.* **D68** (2003) 014013, [[hep-ph/0212346](#)].
- [33] **BaBar** Collaboration, J. P. Lees et al., *Measurement of the $\gamma^*\gamma^* \rightarrow \eta'$ transition form factor*, *Phys. Rev.* **D98** (2018) 112002, [[arXiv:1808.08038](#)].
- [34] A. Nyffeler, *Hadronic light-by-light scattering in the muon $g - 2$: A New short-distance constraint on pion-exchange*, *Phys. Rev.* **D79** (2009) 073012, [[arXiv:0901.1172](#)].
- [35] A. Gorsky and A. Krikun, *Magnetic susceptibility of the quark condensate via holography*, *Phys. Rev.* **D79** (2009) 086015, [[arXiv:0902.1832](#)].
- [36] M. Hoferichter, B.-L. Hoid, B. Kubis, S. Leupold, and S. P. Schneider, *Dispersion relation for hadronic light-by-light scattering: pion pole*, *JHEP* **10** (2018) 141, [[arXiv:1808.04823](#)].
- [37] G. Colangelo, M. Hoferichter, M. Procura, and P. Stoffer, *Dispersion relation for hadronic light-by-light scattering: theoretical foundations*, *JHEP* **09** (2015) 074, [[arXiv:1506.01386](#)].